STUDY OF FACTORS AFFECTING THE SUCCESSFUL RECOVERY OF FIXED-WING UAVS ONBOARD SURFACE VESSELS

F.C. Wong[*], F. Veilleux[†], R. Lee[‡] and E. Gagnon[*]

A study was undertaken to identify the parameters that affect successful ship recovery of fixed-wing UAVs. The study focused on how the airwake, UAV flight characteristics and autopilot characteristics interacted along the UAV's trajectory to allow or to hinder a successful recovery. The analysis consisted of a series of Monte Carlo runs where the UAV passed through a virtual airwake towards a hypothetical capture device. The trajectory, miss distance and control surface effort were used to calculate performance metrics. It was found that lower frigate speed, higher UAV speed and wider off-beam location of the capture device all contributed to increased probability of successful recovery.

INTRODUCTION

Uninhabited Aerial Vehicles (UAVs) are generally becoming more prevalent in military operations for dull, dangerous and dirty tasks. Maritime forces have a particular need for ship-based UAVs to extend their observation horizon and to increase their situational awareness. The principle logistical problem for ship-based UAVs has been the safe and reliable recovery of the platform. The importance of this problem was highlighted in a conference entitled "Launch and Recovery of Manned and Unmanned Vehicles from Surface Platforms: Current and Future Trends" that was sponsored by the American Society of Naval Engineers in 2008[1].

Launching of UAVs from ships has not generally been a problem because the platform accelerates from a turbulent air environment near the ship deck and superstructure into steady air as it flies away from the ship. Past launch methods used some form of rocket-assisted take-off technique[2] or bungee launch[3]. Several developmental programs for launchers based on pneumatic, electromagnetic or linear induction motor technology are currently receiving significant funding from the UK and US governments[4].

Recovery, on the other hand, requires the platform to decelerate from steady air into turbulent air. The combination of slower airspeeds and increased turbulence makes ship-based UAV recovery an operational challenge particularly in foul weather and high sea states. If UAVs are to be used on board ships, a reliable method is needed to recover the UAV. Three systems, to date, have been developed and are being tested in the USA[5]. The first system, from Geneva Aerospace, uses an arresting cable[6,7]. The references indicate that most of the Geneva effort is focused on the guidance system rather than the cable arresting system. The second system, from Engineered Arresting Systems Corp. (ESCO), employs an energy absorbing nylon net to decelerate and capture a UAV[8]. This system can be adapted to any size of aircraft as evidenced by the company's prod-

[*] Defense R&D Canada, Tel: (418) 844-4000 x4200, Fax: (418) 844-4502,
e-mail : franklin.wong@drdc-rddc.gc.ca , website : www.valcartier.drdc-rddc.gc.ca
[†] AEREX Avionic Inc.
[‡] National Research Council - Institute of Aerospace Research

ucts for arresting manned military aircraft. The obvious disadvantage of a net system is its size. However, a net can be hung over the side of a ship so that it does not occupy deck space. The third system is the Boeing/Insitu Skyhook that is developed specifically for the company's ScanEagle UAV[9]. Autonomous capture is accomplished by guiding the ScanEagle towards a suspended cable. A hook at the wing tip latches onto the cable as long as some part of the wing initially engages the cable.

All the UAVs used to date to evaluate concepts for the maritime environment have been platforms initially developed for the Army or Air Force environments. Thus 'dry land' recovery techniques like those previously described have been studied. Other companies have proposed seaplane UAVs[10] to obviate the need to land on a ship. Their concept envisions a UAV landing nearby the ship before being winched back on board. Detractors of this concept cite the difficulties that a seaplane would have landing in high sea-states and the additional manpower and equipment that is needed to physically attach a recovery line to the seaplane.

This study was undertaken to understand the parameters that affect successful fixed-wing UAV ship recovery using 'dry land' techniques. It focuses on how the airwake environment, UAV flight characteristics and autopilot characteristics interact along the UAV's final approach towards a hypothetical capture device to allow or to hinder successful recovery.

BACKGROUND AND SCOPE

A HALIFAX class frigate was selected as the candidate ship for this study. Figure 1 shows the flight deck and hangar geometry for the frigate. The Helicopter Hauldown and Rapid Securing Device (HHRSD) "bellmouth" through which the hauldown cable passes is located approximately 14.0 metres aft of the helicopter hangar door on the ship's longitudinal centreline.

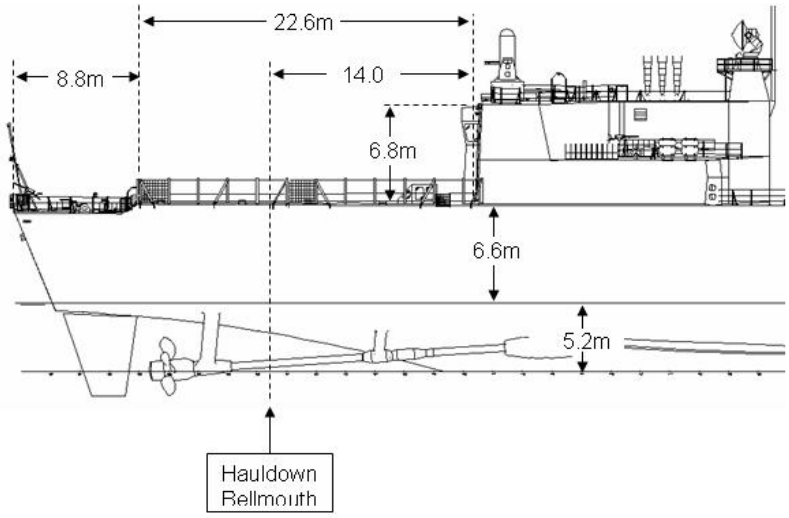

Figure 1. Flight deck and hangar geometry for HALIFAX class frigate. Flight deck width, front = 16.4m. Flight deck width, rear = 14.4m.

Six emplacements on the frigate's flight deck were selected as candidate locations for a hypothetical capture device: T1) 5 m aft of the hangar door on the ship centreline, T2) 14 m aft of the hangar door on the ship centreline, and T3) 14 m aft of the hangar door and offset on the starboard side by 4 m, T4) 14 m aft of the hangar door and offset on the port side by 4 m, T5) 14 m

aft of the hangar door and offset on the starboard side by 8 m, and T6) 14 m aft of the hangar door and offset on the port side by 8 m. The capture device was assumed to be 3.4 m above the flight deck.

For the purposes of the study, the frigate was assumed to have a displacement of 4440 tons which corresponds to an operational light condition. Previous studies of the airflow around a frigate showed that a port-side relative wind, or more specifically, a Red30 condition was a challenge due to the high turbulence with strong unsteady vortices and shear layers[11,12]. Therefore, it was decided that the two basic wind conditions of interest for this study would be the Red30 and Red45 wind conditions.

It was assumed that the frigate would sail at either 10 kts or 15 kts. To obtain the Red30 condition for a frigate sailing at 15 kts, the frigate must sail on a course of 060 with a freestream wind coming from the North at 15 kts. A Red30 condition is obtained for a frigate sailing at 10 kts when it is on a course of 050 with a freestream wind coming from the North at 13.2 kts. To obtain the Red45 condition for a frigate sailing at 15 kts, it must sail on a course 090 with a freestream wind coming from the North at 15 kts. A Red45 condition for a frigate sailing at 10 kts is obtained when it is on a course of 074 with a freestream wind coming from the North at 14.4 kts. Figure 2 shows the relationship between the ship course and wind directions.

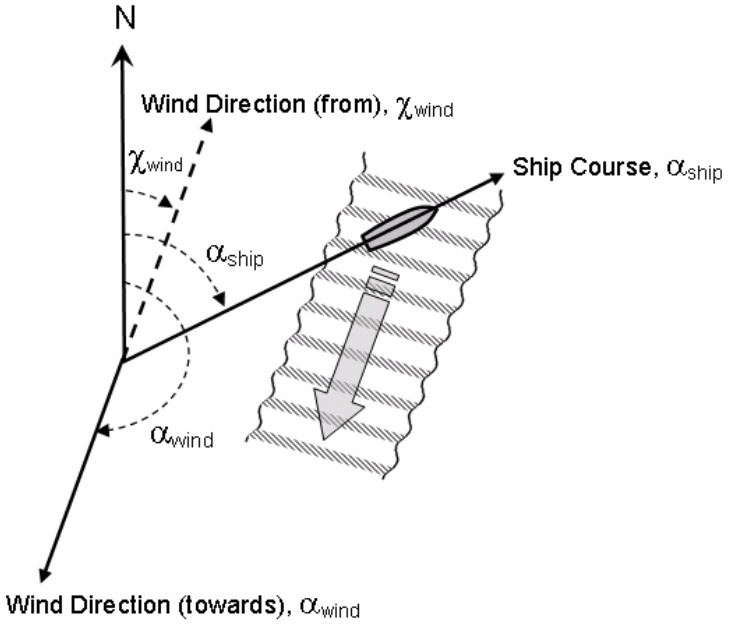

Figure 2. Coordinate system relating wind, wave and ship course directions. The UAV maintains a course equivalent to the ship course.

An Aerosonde was selected as the candidate UAV and was assumed to fly with an airspeed of 54 kts (100 kmh) or 76 kts (140 kmh) along the same course as the frigate. Table 1 shows the relative ship speeds, UAV airspeeds and directions selected for the parametric analyses. The table has been organized by ship course, $\alpha_{ship/earth}$, then by wind ground speed, $V_{wind/earth}$, then by ship ground speed, $V_{ship/earth}$, and finally by UAV airspeed, $V_{UAV/wind}$.

Table 1: Relative ship and UAV speeds and directions for selected wind speed ship course, ship speed and UAV speed								
Condition	1	2	3	4	5	6	7	8
$\alpha_{ship/earth}$ (deg)[a]	060	060	050	050	090	090	074	074
$V_{wind/earth}$ (kts)[a]	15	15	13.2	13.2	15	15	14.4	14.4
$V_{ship/earth}$ (kts)[a]	15	15	10	10	15	15	10	10
$V_{wind/ship}$ (kts)[b]	26.0	26.0	22.8	22.8	21.2	21.2	20.2	20.2
Relative wind[b]	Red30	Red30	Red30	Red30	Red45	Red45	Red45	Red45
$V_{UAV/wind}$ (kts)[a]	54	76	54	76	54	76	54	76
$\theta_{UAV/wind}$ (deg)[b]	13.9	9.9	12.3	8.8	16.1	11.3	15.5	11.0
$V_{UAV/earth}$ (kts)[b]	45	67	43	65	52	75	48	70
$V_{UAV/ship}$ (kts)[b]	30	52	33	55	37	60	38	60

Note: [a] signifies parameters that were specified, [b] signifies parameters that were calculated. Parameters A/B are read as 'parameter of A relative to B'. For example, $V_{wind/earth}$ is read as 'velocity of wind relative to earth coordinates' or, in other words, wind ground speed.

GENERATION OF AIRWAKE DATA

In the past several years, advances in computing power and algorithms have permitted computations of spectrally-correct airwakes suitable for use in real-time simulations of flight vehicles. Navier-Stokes or Lattice-Boltzman codes are required in order to produce time-accurate information[11]. In the present context, the NRC Institute of Aerospace Research chose to run PowerFLOW©, a Lattice-Boltzmann approach. PowerFLOW tracks discrete particles moving and colliding in a cubic lattice at discrete time steps. The algorithm is explicit and stable by nature. Macroscopic quantities such as density and velocity can be determined by averaging various properties of the particles occupying a given lattice cell at any given time. The simulation of high Reynolds number flows is handled using a Very Large Eddy Simulation (VLES) turbulence model and modified wall functions.

The analysis was set up to run for 90 seconds after any initial transients had been damped. PowerFLOW uses the concept of virtual "probes" to allow the user to sample the time history of the flow at any given location (x - longitudinal, y - starboard, z - up) in the flow field. In the pre-

sent case, a series of probes were placed along the axis of the ship ($y = 0$) for $x = -5$, –4, –3, –2, –1, 0, 1, 2, 3, 4, 5, 6, 7, 8, 9, 10, 12.5, 15, 17.5, 20, 22.5, 25, 27.5, 30, 35, 40, 45, 50, 70, 90, 120, 140, 180 m where $x = 0$ m corresponds to the bellmouth location (Figure 1). The z-coordinate at $x = 5$ m was 3 m. All other z-coordinates were defined from this one point based on a glide slope of –6 degrees.

At each of these axial locations, an array of 43 probes was arranged on a rectangular grid. Twelve of these points were laterally displaced at $y = \pm 2, \pm 4, \pm 6, \pm 8, \pm 10, \pm 12$ m relative to the local reference, six of these were vertically displaced at $z = \pm 2, \pm 4$, and ± 6 m relative to the local reference coordinate and four of these were placed at the corners of the rectangle corresponding to $y = \pm 12$ m and $z = \pm 6$ m. The remaining probe points were placed on diagonal trajectories within the grid (see also Figure 4). The probes located below the flight deck were ignored. Note that the probe sampling rate varied depending on the longitudinal location of the probes. This strategy allows more sampling to occur where flow gradients and thus turbulence are highest. The probes were sampled at approximately 200 Hz over the flight deck with the rate decreasing to about 15 Hz in the far field where the turbulence is minimal. Figure 3 shows 10 seconds of typical airwake data taken at $x = y = 0$ at varying heights of z.

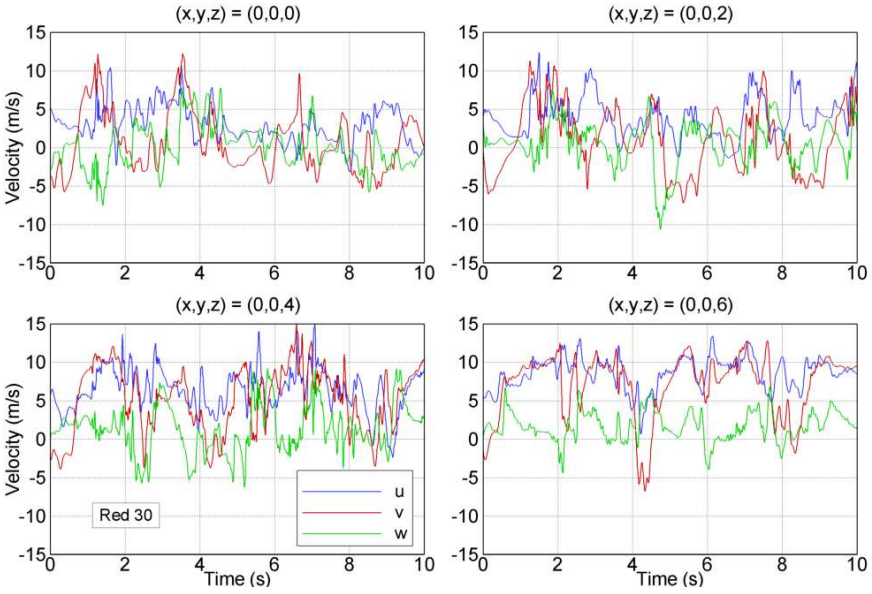

Figure 3. Typical airwake data at x = y = 0 at varying heights of z (velocities u (x-dir) in blue, v (y-dir) in red, w(z dir) in green).

In order to create an "endless" loop of airwake data, the 90 s time history from PowerFLOW was fed into a Matlab program that used cubic spline interpolations to add 25 points at the end of the airwake time history for the velocity components u, v and w at each probe location at the same sample rate. The 25 additional points at the end were determined so that the first few points of this data formed a smooth transition including first derivative compatibility to the end of the time history, and the last few of these points formed a smooth transition including first derivative compatibility to the beginning of the time history. In this way, an endless loop was created so that simulated flights could be initiated at any time without concerns about discontinuities in the airwake data.

Data were calculated for Red30 and Red45 wind conditions with a freestream wind speeds that corresponded to frigate speeds of 10 or 15 kts. A "Red" wind is a wind coming from the port side of the bow. The resultant velocity vectors were scaled to relative wind magnitudes shown in Table 1.

Contours of velocity ratio and turbulence intensity in the *y*-*z* plane of the time-averaged flow field are depicted in Figure 4 and Figure 5 for a Red30 and a Red45 winds, respectively. For brevity of presentation, the velocity ratio and turbulence intensity encapsulate total quantities, *i.e.*, the norm of the *x*-, *y*- and *z*-component quantities. Both ratios use the freestream velocity as a reference. The blended contours of velocity ratio and turbulence intensity were developed with Kriging interpolation. The velocity-ratio vectors are of equal length and serve to indicate directionality; vectors that appear to be shorter are in fact directed out of the *y*-*z* plane.

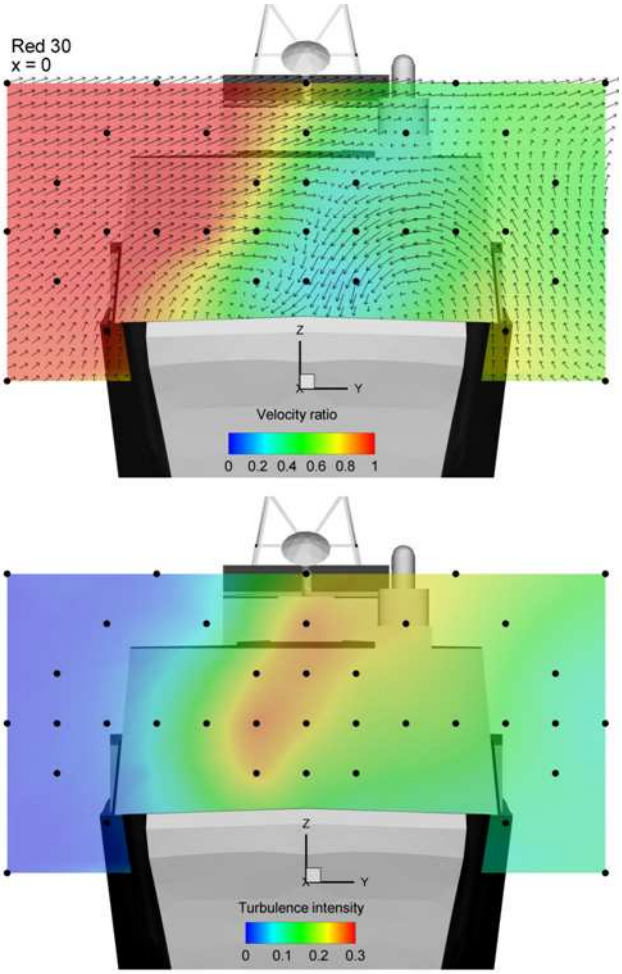

Figure 4. Contours of velocity ratio and turbulence intensity of the time-averaged flow field in the ship coordinate system at x=0 for Red30 wind. Black dots represent the locations of the virtual probes.

In Figure 5, the velocity field reflects an asymmetric airwake. Of particular note is the downward tendency of the flow in the airwake. Also, a velocity ratio of approximately 0.5 – representing a velocity deficit – dominates most of the flight deck width. Numerous vectors show signs of out-of-plane flow. On the windward side of the flight deck, the turbulence intensity is zero which is expected being that it is in the airwake of the ship superstructure. The turbulence intensity on the leeward side is reasonably constant at 0.1. In between, over the flight deck, there is a band of elevated turbulence intensity, ranging from 25% to 30%, that arises from the shear layer emanating from the windward vertical walls of the hangar. In Figure 5, the increase in wind direction leads to a shift of the airwake features to the leeward side. In addition, the windward vortex that forms on the flight deck is more strongly defined; also, a large region of near-freestream flow is apparent above the windward half of the flight deck. The corresponding turbulence intensity results reflect a similar shift across the flight deck. For further discussions on flow topology over a frigate-like shapes, the reader is referred to Reference 12.

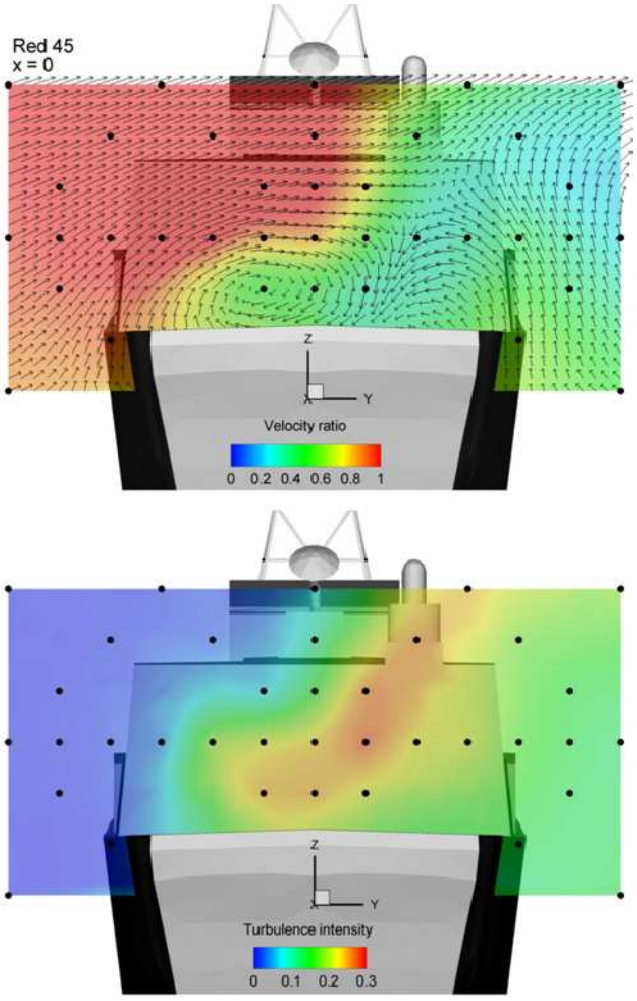

Figure 5. Contours of velocity ratio and turbulence intensity of the time-averaged flow field in the ship coordinate system at x=0 for Red45 wind. Black dots represent the locations of the virtual probes.

HARDWARE IN THE LOOP FACILITY

Description

A hardware in the loop (HWIL) facility is used for the parametric study. In this facility (Figure 6), Computer 1 reads the command signals sent by the autopilot to the UAV actuators, namely the elevator, ailerons, rudder and throttle, and translates them to actuator angles and throttle fraction before providing them to the 6DOF UAV model. The states of the 6DOF UAV model are updated, taking into account the airwake and wind effects. The corresponding sensor signals are generated and returned to the autopilot through an interface board. Computer 1 also updates the state of the ship which is affected by the sea state. Computer 2 is used to run the ground control station software. This computer is connected to the autopilot using the same communication link that is used to perform real flights. X-Plane is used to obtain a 3D view of the simulation. All models are implemented within Simulink and are run with xPC Target.

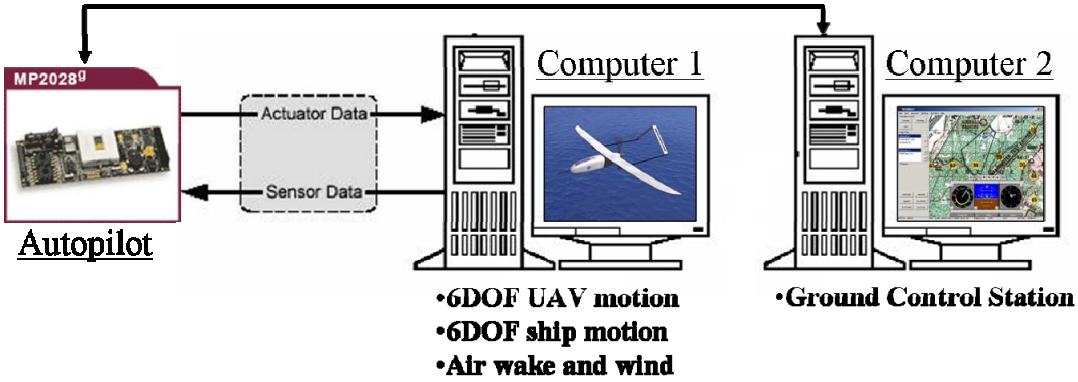

Figure 6. ***Hardware-in-the-loop simulation test bed.***

The 6DOF UAV model is parameterized to reproduce the behaviour of an Aerosonde UAV. This model expresses aerodynamic forces and moments based on stability and control derivatives. The aerodynamic forces and moments are summed with the forces and moments generated by the propulsion and fed into the equations of motion to compute the UAV states. The 6DOF UAV model was developed with the Aerosim Blockset from Unmanned Dynamics.

The HWIL autopilot is the MP2028 from MicroPilot. The MP2028 allows GPS waypoint navigation with altitude and airspeed hold. It allows completely independent operation including autonomous takeoff, bungee launch, hand launch and landing. The MP2028 is fully integrated with 3-axis gyros/accelerometers, Global Positioning System (GPS), pressure altimeter and pressure airspeed sensors. With the MP2028, it is possible to perform extensive data logging and telemetry.

Implementation of Airwake Data

The airwake data received from the PowerFLOW analysis are processed before their implementation. To be able to get the wind velocity at any position behind the ship, the wind data are placed in a four dimensional lookup table that order the three velocity vector components as a function of time. The lookup table outputs are generated using linear interpolation to regularize the time increments. All data are loaded into memory so that there is no delay in the real-time calculations.

The set of airwake data form a corridor through which the UAV flies. The corridor position in earth-coordinates is synchronized with the movement of the ship so that its position relative to the ship's position is always constant.

The freestream wind and direction are entered separately from the airwake data in the simulation environment. As such, a discontinuity exists between the freestream and airwake data at the lateral boundaries of the airwake corridor. The discontinuity at the entrance of the corridor is minimal because the corridor entrance extends far enough away from the frigate and allows matching between the freestream and airwake data at that point in space.

Scenario Set-up

While the UAV is in the airwake corridor, data are logged at 10 Hz. The data captured included UAV position and attitude, airspeed, angular rates, distance with respect to the ideal trajectory in the corridor, and servo commands.

The airwake data represents an airwake corridor aft of the frigate with a slope of 6 degrees. To simplify the simulation, the corridor was assumed to be horizontal without any slope otherwise it would have been necessary to calculate vertical offsets for each data plane at each time step as the UAV flew through the airwake.

When the autopilot is in autonomous mode, the UAV simply follows a list of waypoints that is saved in the autopilot memory. These waypoints are placed in a manner such that the UAV is able to make a circuit through the ship, capture device and airwake corridor positions (Figure 7). The circuit is a way to make consecutive passes for the Monte Carlo study without manually repositioning the UAV each time.

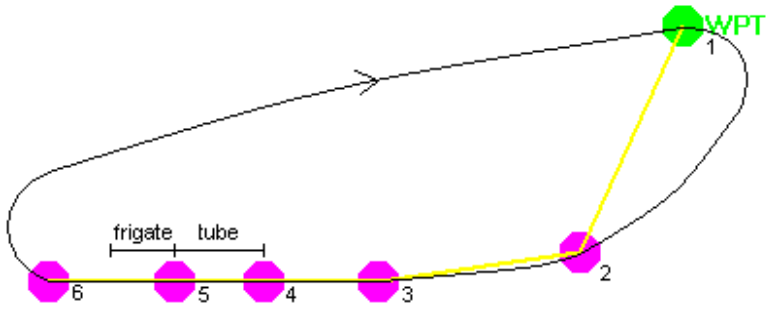

Figure 7. W*aypoint configuration chosen for Monte Carlo analysis.*

To get a representative simulation, the UAV has to arrive parallel to the corridor centreline at the corridor entrance. Thus, waypoints 3 to 6 were placed in a straight line. Waypoint 4 was placed at the corridor entrance while waypoint 5 represented the capture device position. Waypoint 6 forced the UAV to continue past the frigate before a turn was initiated towards waypoint 1 while waypoint 2 aided in the initial alignment of the UAV with waypoint 3. All waypoint positions are referenced relative to the frigate's time-varying position.

Parametric Study

There are several parameters that affect UAV recovery on board a ship. Assuming that the freestream wind is coming from a northerly direction, the course of the frigate should have a great influence, since the relative wind that the UAV experiences is a vector sum of the frigate and wind velocity vectors relative to earth. Another parameter that should affect UAV recovery is the UAV's airspeed. Airspeed not only affects the time to the capture device, it also affects the

amount of control authority generated by the UAV's control surfaces. Furthermore, the position of the capture device (also called target in this study) on the frigate deck changes the trajectory followed by the UAV, and consequently, the airwake effects on the vehicle during its approach and recovery.

The Monte Carlo analysis consisted of 50 passes of the UAV through the airwake corridor for each scenario in Table 1 to obtain statistically meaningful data. At an airspeed of 54 kts, the UAV takes approximately 12 s to fly through the 180 m long airwake corridor. The stochastic nature of the airwake was reproduced naturally by the endless loop of airwake data and the stochastic times at which the UAV entered in the airwake corridor.

The ability of the autopilot to guide the UAV to the target was evaluated numerically by calculating the average location in y and z coordinates, and the standard deviation in y and z where the UAV passed the vertical plane of the capture device. The standard normal distribution equations were used for statistical analysis[13]. The difficulty for the UAV to maneuver in the airwake corridor was evaluated by the control surface effort in terms of degrees in this study because surface deflection was a readily available parameter in the simulation.

RESULTS AND DISCUSSION

To gain a general appreciation of the influence that Frigate Speed, UAV Airspeed and Target Location have on landing accuracy, the average miss distance and its standard deviation have been plotted on a single graph for all scenarios for each parameter. Figure 8 and Figure 9 show the miss distance results for Frigate Speed when sorted by Red30 and Red45 wind conditions. A rectangle representing a 6 m x 6 m capture device is included for reference purposes. It can be seen in Figure 8 that a slower frigate speed of 10 kts helps increase the chances of recovery since there are fewer runs that fall outside the bounds of the fictitious capture device. The width of the error bars indicate the probable capture position at 68% of the time assuming the data is normally distributed[13]. The errors bars for the Frigate Speed of 10 kts are qualitatively smaller for both Red30 and Red45 wind conditions indicating that the UAV is better able to handle the turbulence when the frigate is sailing at the slower speed. The higher frigate speed has a greater tendency to push the recovery location onto the deck presumably because the downdraft over the hanger is stronger.

Figure 10 and Figure 11 illustrate the global effect of UAV speed on recovery success. When the UAV speed is lower, it has more difficulty arriving within the bounds of the fictitious capture device. The Red30 wind condition created more problems as shown by the greater number of run markers falling below the capture device bounds in Figure 10. At the higher UAV speed, the run markers are tightly grouped along a vertical line on the port side of the center line. The slower UAV speed resulted in a larger variability of the recovery location, particularly in the Red30 wind conditions, and leads one to conclude that slower speed leaves the UAV vulnerable to the effects of the strong downdraft off the hangar.

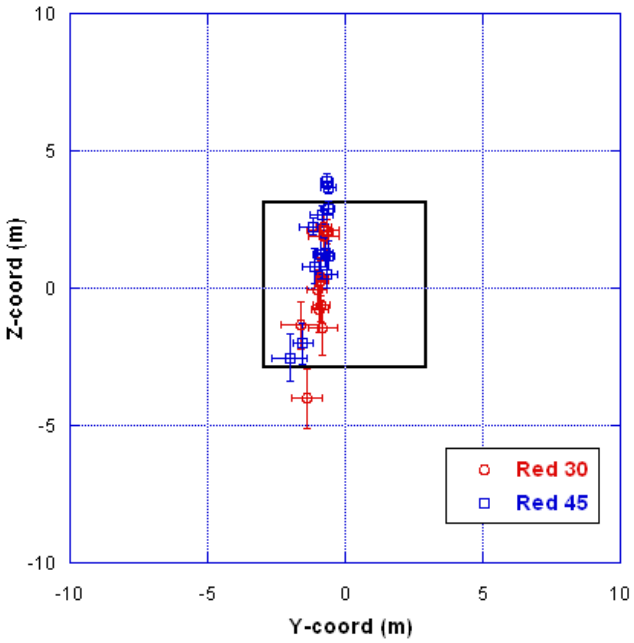

Figure 8. Average and standard deviation of miss distances for all runs where frigate speed is 10 kts. Rectangle represents fictitious 6 m x 6 m recovery net.

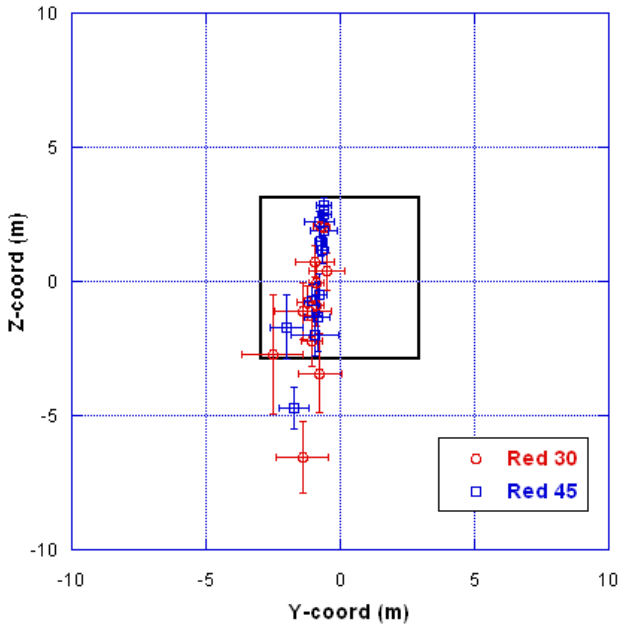

Figure 9. Average and standard deviation of miss distances for all runs where frigate speed is 15 kts. Rectangle represents fictitious 6 m x 6 m recovery net.

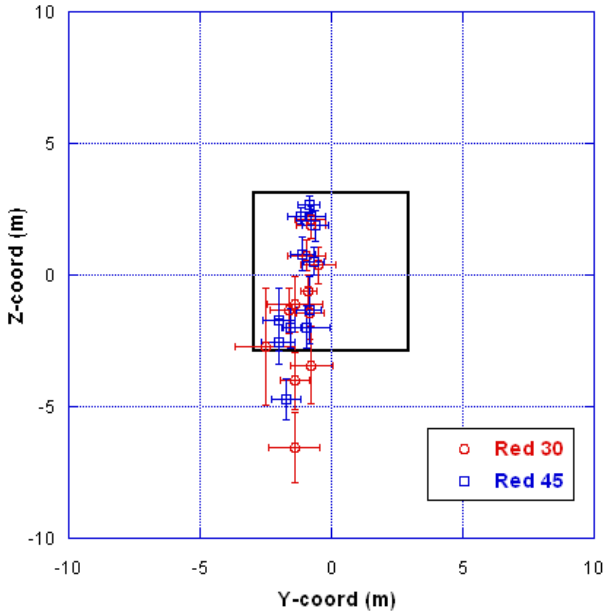

Figure 10. Average and standard deviation of miss distances for all runs sorted where UAV speed is 100 km/h (54 kts). Rectangle represents fictitious 6 m x 6 m recovery net.

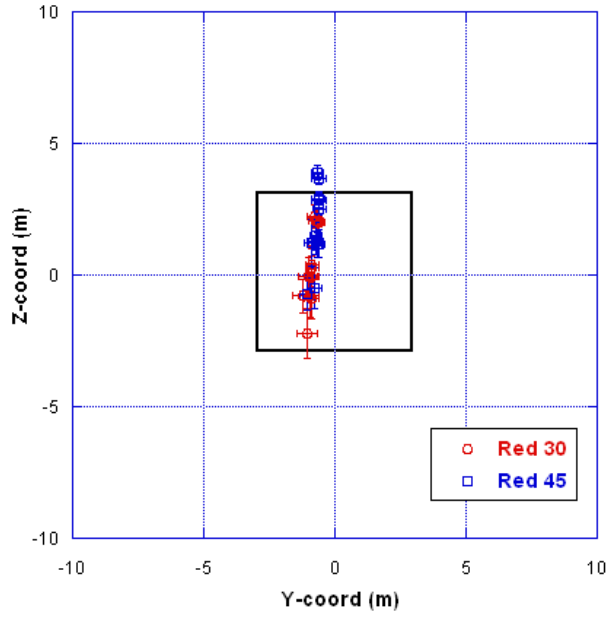

Figure 11. Average and standard deviation of miss distances for all runs where UAV speed is 140 km/h (76 kts). Rectangle represents fictitious 6 m x 6 m recovery net.

Figure 12 shows the miss distance results as a function of the capture device locations under Red 30 wind conditions. From the graph, the location [5, 0] m, ie. 5 m aft of the hangar door on the centerline, has run markers tightly grouped within the bounds of the capture device. The locations [14, -4] m and [14, -8] m, ie. on the port side, may be considered adequate since its run markers fall within the capture device bounds. These locations, though, have a greater dispersion. The location [14, +8] m, ie. on the starboard side, may be adequate under certain restricted conditions since one of the run marker has its error bands falling outside the capture device bounds. The locations [14, 0] m and [14, +4] m have run markers falling outside the bounds suggesting that these locations are not appropriate for UAV recovery unless there are restrictions on the UAV or frigate speed.

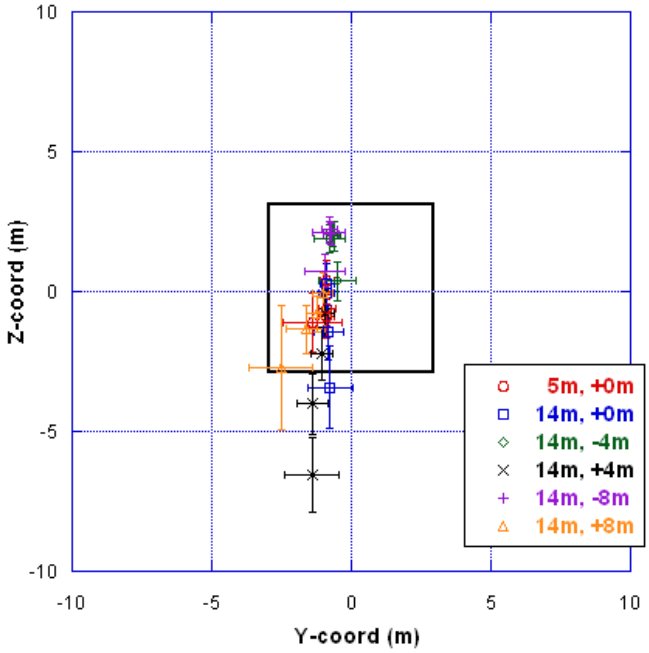

Figure 12. Average and standard deviation of miss distances for all runs with Red30 wind conditions. Rectangle represents fictitious 6 m x 6 m recovery net. Positive y is on the starboard side.

The groupings for the Red45 wind condition, Figure 13, are tighter indicating that this wind condition imposes fewer constraints on the location of the capture device on the deck. In this case, the locations [5, 0] m and [14, 0] m, fall inside the capture device bounds. Location [14, +8] m is marginally acceptable because one of the run marker's error bounds falls outside the device bounds. With run markers falling outside the device bounds, locations [14, -4] m, [14, +4] m, and [14, -8] m would not be considered acceptable unless limitations were placed on the frigate or UAV speeds.

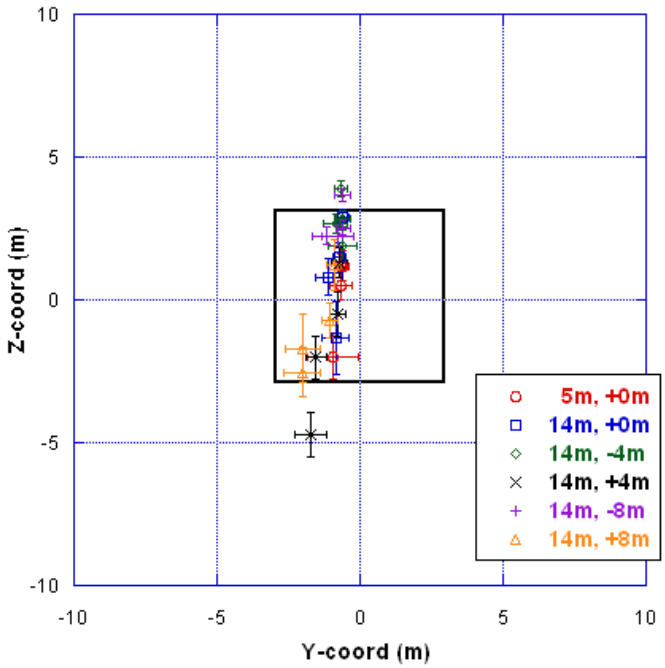

Figure 13. Average and standard deviation of miss distances for all runs with Red45 wind conditions. Rectangle represents fictitious 6 m x 6 m recovery net. Positive y is on the starboard side.

Figure 8 through Figure 13 suggest that the dependency of miss distance on the parametric study parameters is more subtle. To extract this dependency, the runs of each scenario were grouped and then averaged to better understand what influence, if any, the study parameters had on miss distance and control effort. The results of this exercise, which are not presented here, allowed several observations to be made:

1. On the basis of the average miss distance for all runs, Red30 wind conditions (miss of [-1.01,-0.50] m) caused the same level of difficulty as the Red45 wind conditions (miss of [-0.94, +0.71] m).
2. Average miss distance is smaller when frigate speed is lower. For example, at Red30, 10 kts frigate speed has an average miss distance of [-0.95, +0.06] m while 15 kts frigate speed has an average miss distance of [-1.07, -1.05] m.
3. At Red30 conditions, a higher UAV speed of 76 kts, where an average miss distance is [-0.87, +0.35] m, results in improved chances of recovery over a lower UAV speed of 54 kts where an average miss distance is [-1.15, -1.34] m. The statistical results for the Red45 conditions are ambiguous.
4. The recovery or target position at [5, 0] m has the lowest average miss distance for the Red30 conditions ([-1.00, -0.55] m) and the Red45 conditions ([-0.72, +0.22] m).
5. The recovery or target positions at [14, 0] m and [14, -8] m have average miss distances that are generally lower than the other recovery positions except for the [5, 0] m position.
6. The recovery or target positions at [14, -4] m and [14,+8] m have average miss distances that are generally greater than the other recovery positions.

7. The numerical results for the [14, +4] m average miss distance are ambiguous on the basis of wind conditions although it is clear that the [14, -4] m average miss distances are lower on a comparative basis.
8. On the basis of the average total control surface effort for all runs, Red30 wind conditions (effort of 1233 deg/pass) require slightly more effort than Red45 wind conditions (effort of 1162 deg/pass).
9. Transiting through the airwake requires much more effort to control altitude than heading. For example, in Red30 wind, the average elevator effort is 988 deg/pass compared to the average aileron and rudder effort of 185 deg/pass and 60 deg/pass, respectively.
10. More control effort was applied at faster UAV speed. For example, in Red30 wind, at UAV speed of 54 kts, an average total effort of 715 deg/pass was applied. At UAV speed of 76 kts, an average total effort of 1752 deg/pass was applied.
11. A higher control effort was applied to maneuver the UAV to the recovery position [5, 0] m than the other locations. For example, in Red30 wind, the average effort for [5, 0] m was 1465 deg/pass. The average total effort for the other positions was roughly 1200 deg/pass.

CONCLUSIONS

The objective of this study was to understand the parameters that influence successful ship recovery of a fixed-wing UAV through the use of a UAV hardware-in-the-loop (HWIL) facility. Results have been generated using CFD and UAV simulation technologies. The simulations were used to indicate trends needed for successful recovery rather than be used as a predictive tool to produce expected performance results.

The frigate speed, which partially controls the strength of the turbulence behind the hangar, had a marked effect on the average UAV miss distance. More scatter in the recovery locations was observed for a frigate traveling at 15 kts than for a frigate traveling at 10 kts in Red30 and Red45 wind conditions. In both cases, it was interesting to observe that the recovery locations were quite tightly grouped in the beam-direction while the grouping in the altitude direction was more scattered. A higher average actuator effort was required for a slower frigate speed in Red30 wind conditions while lower average actuator effort was required for Red45 wind conditions.

The UAV airspeed, which influences time-to-target and air vehicle manoeuvrability, produced lower average miss distance and lower dispersion at higher UAV airspeeds. Red30 winds caused greater dispersion of recovery locations than Red45 winds at the lower UAV airspeed. In terms of actuator effort, higher UAV airspeeds required higher average actuator effort.

For the capture device or target locations, the target located on the ship centerline at 5 m aft of the hangar generally had the lowest average miss distance. Targets located on the port side of the ship generally had lower average miss distances and dispersions than targets located on the starboard side. Red30 winds caused greater dispersion of recovery locations at all target locations than Red45 winds. Less actuator effort was required to fly to port side target locations.

Future studies will examine techniques to minimize the effects of the airwake on the UAV landing trajectory.

REFERENCES

[1] "Launch and Recovery of Manned and Unmanned Surface Platforms 2008" sponsored by the American Society of Naval Engineers, Annapolis, Maryland, May 2008; http://www.navalengineers.org/EventArchives/LR2008/LR2008HP.html, accessed 20 July 2009.

[2] Ashworth, P., "Unmanned Aerial Vehicles and the Future Navy", Working Paper No. 6, Royal Australian Navy, May 2001; http://www.navy.gov.au/spc/workingpapers/, accessed 13 July 2007.

[3] Patterson, M.C.L., Mulligan, A.C., "Unmanned Air Vehicle Requirements - Meeting the Need of the Warfighter", Advanced Ceramics Research, presented at Hawaii Technology Enterprise 2006, June 2006; http://www.hitdv.com/TechEnterprise_2006/UAV_Requirements.pdf, accessed 14 July 2007.

[4] Scott, R., "On a wing and a prayer", Unmanned Vehicles, April 2007, pp. 12-15.

[5] Glenn, I., "Options for Canadian Navy Organic UAV Operations", DRDC Ottawa CR 2006-168, July 2006.

[6] Geneva Aerospace, http://www.dawnbreaker.com/vas06/browse.php?angle=browse&b=&viewPageNum=2&viewCatID=0&viewCmdID=0&sortID=0&squery, accessed 14 July 2007.

[7] http://www.dodsbir.net/selections/abs031/navyabs031.htm, accessed 14 July 2007.

[8] Engineered Arresting Systems Corp., http://www.esco.zodiac.com/index.cfm/navid-101, accessed 14 July 2007.

[9] Insitu Inc., http://www.insitu.com/prod_groundsupport.cfm, accessed 14 July 2007.

[10] DRS Technologies, http://www.drs.com/Products/NEPTUNE.aspx?cat=Intel_Tech&subcat=Sub_Cat_22, accessed 23 November 2007.

[11] Zan, S.J., Syms, G.F., and Cheney, B.T. , "Analysis of Patrol Frigate Airwakes", presented at NATO/RTO Meeting on Fluid Dynamic Problems of Vehicles Operating in or near the Air/Sea Interface: RTO-MP-15, Amsterdam, October 1998.

[12] Zan, S.J., "Surface Flow Topology for a Simple Frigate Shape", Canadian Aeronautics and Space Journal, Vol. 47, Issue 1, pp. 33-43, 2001.

[13] CRC Standard Mathematical Tables, 26th ed., CRC Press, Boca Raton, FL, 1981.